International Journal of Geosynthetics and Ground Engineering (2023) 9:70
https://doi.org/10.1007/s40891-023-00488-1

ORIGINAL PAPER

Deformative Response of Sheltering Structures Under the Debris Flow Impact

Domenico Gioffrè[1] · Maria Clorinda Mandaglio[2] · Mariantonietta Ciurleo[3] · Nicola Moraci[4]

Received: 31 March 2023 / Accepted: 30 September 2023 / Published online: 24 October 2023

Abstract

A relevant issue in the development of disaster risk reduction strategies is played by design of mitigation measures aimed at reducing risk to acceptable values. For rapid landslides, such as debris flows, sheltering structures are very common mitigation measures realized in exposed areas that allow to protect elements at risk and to stop flowing mass. For the design of these works, the debris flow–structure interaction mechanism is very important. The paper focuses on the evaluation of debris flow–structure interaction mechanism in earth reinforced embankments based on an uncoupled analysis of the interaction in two flow cases (dominant static and dynamic). In particular, a novel approach to evaluate the horizontal stress distribution at different time of the impact phenomenon along the upstream face height of deformable sheltering structures considering the dominant flow component has been proposed. First, impact force over the time against structure is calculated. Subsequently, assuming that debris flow is completely stopped by embankment according to a scheme of accumulation of material behind the obstacle, the deformative response of different geometrical types of embankment is obtained by FEM numerical analysis for considered flow cases. The results of numerical analyses are discussed in terms of horizontal displacements in different control points in sheltering structures. The analysis showed that the deformative response of two geometries of embankments depends on dominant static or dynamic components of impact force.

Keywords Risk mitigation · Deformable structures · Debris flow–structure interaction · FEM analysis

Introduction

Debris flows are rapid landslides in which a large volume of a highly concentrated viscous soil–water mixture moves in a steep channel or along a slope. They are sharp transient phenomena characterized by periodic surges of soil and water (thoroughly mixed) separated by periods of relatively low or zero flow. The channeled debris flow may initiate by a shallow sliding failure, debris avalanche or rock fall from a steep slope with generally small initial mobilized volume. During its movement through the channel, the landslide mass accelerates and entrains water and soil increasing its volume. Debris flow can cause considerable damage, have relevant societal impact, and represent a permanent hazard in many regions especially at the toe of the hills where they usually accumulate and where people live (element at risk) because the extensive flat areas favor intense urbanization. For these phenomena, the quantitative assessment of susceptibility by means of physically based models represents a key step for risk analysis and for risk mitigation measures [1–4]. Regarding mitigation works, the attention of

✉ Maria Clorinda Mandaglio
mmandaglio@unisa.it

Domenico Gioffrè
domenico.gioffre@unipv.it

Mariantonietta Ciurleo
mariantonietta.ciurleo@cnr.it

Nicola Moraci
nicola.moraci@unirc.it

[1] Department DICAr, University of Pavia, Via Ferrata, 3, 27100 Pavia, PV, Italy

[2] Department DICIV, University of Salerno, Via Giovanni Paolo II, 132-84084 Fisciano, SA, Italy

[3] National Research Council of Italy, Research Institute for Geo-Hydrological Protection (CNR-IRPI), Rende, CS, Italy

[4] Department DICEAM, Mediterranea University of Reggio Calabria, Via Graziella, Località Feo di Vito, 89122 Reggio Calabria, Italy

several scientists focuses on debris flow sheltering structure (deformable or rigid) design to locate in the exposed areas. These structures allow to protect the element at risk reducing the runout distance, the debris velocity, and to stop the debris flow decreasing residual destructive power (Fig. 1).

The design of these "debris-arresting" structures is based on the estimation of the magnitude of the design event, debris flow mobility, and impact load. According to main international codes and guidelines [5], the impact force exerted by flowing material on a structure is estimated mainly using empirical formulas. Among these, the most commonly used approaches are the following models:

- Fluid-based, hydrostatic and hydrodynamic models [6–8];
- Hybrid, a combination of previous ones [9];
- Discrete element approach [10].

In the hydrostatic approach, the impact force depends on debris flow height and soil unit weight, and the pressure profile with depth on the structure is linear (triangular shape). In the hydrodynamic approach, the impact force depends on debris flow velocity and it is schematized as a constant pressure profile (rectangular shape) on the structure.

A simplified relationship of a fluid-based model proposed by Gioffrè et al. [9] was proposed to evaluate the impact force with time (F) by adding the static force (F_{stat}) to that dynamic (F_{dyn}) one.

Calvetti et al. [10] proposed a new formulation of impact force based on results of discrete element method analysis that is able to take into account the geometry, the Froude number, and the porosity of the flowing mass.

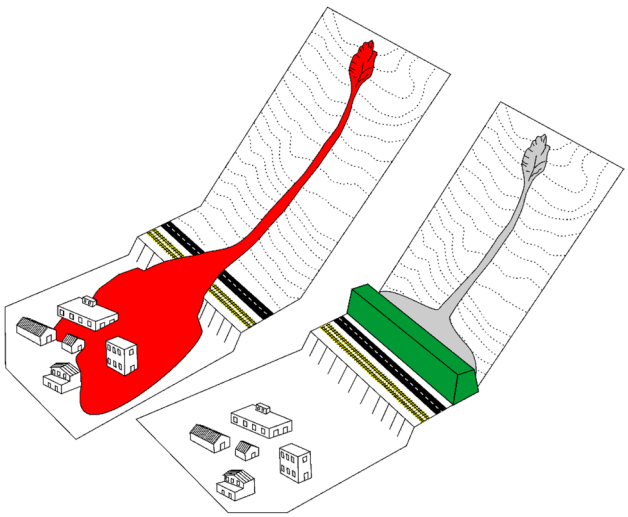

Fig. 1 Scheme of the effect of the sheltering structures as mitigation measures against debris flow

Debris flow–structure interaction mechanism is an actual issue and the complexity of behavior of flow-like material against the structure is also affected of the relative stiffness between debris flow mass and protective structure.

Independently on the adopted approaches, the most part of the authors estimates the maximum impact force acting on the structure without considering the evolution with time of this force and its application position on the sheltering structure. Some researchers [11–14] have proposed a simplified approach in which the position of force application is generally chosen according to the assumed pressure profile along the structure. The evolution with time of the accumulation area behind the protective structure is neglected assuming an equivalent rectangular solid-like body that it is supposed to be completely stopped by the sheltering rigid structure. In this context, the paper proposes an approach to analyze debris flow–structure interaction mechanism for deformable sheltering structures. The novelty of the approach is to evaluate the impact pressure against sheltering structure at any instant of time of the phenomenon and along the upstream face height of the deformable sheltering structure depending on the dominant flow component. To obtain a simple design methodology for these structures, an uncoupled analysis of landslide structure interaction is developed. In particular, the impact force over time (static and dynamic components) on the structure is calculated considering the variation of debris flow velocity and thickness over time obtained by numerical simulations of landslide propagation. Consequently, static and dynamic components of impact force change both in value and application position along upstream face of sheltering structure. Based on the estimation of two components of impact force and on a conceptual scheme of accumulation of material behind the obstacle, deformative response of sheltering structure is obtained by FEM numerical analysis.

Materials

Considering that debris flows are dynamic phenomena, the evolution with time of the impact force has been adequately taken into account for the evaluation of the distribution of pressures on the sheltering structure.

A simplified relationship of a fluid-based model proposed by Gioffrè et al. [9] has been used to calculate the impact of force with time (F) by adding the static force (F_{stat}) to that dynamic one (F_{dyn}) at different times of the impact, as follows:

$$F(t) = F_{stat}(t) + F_{dyn}(t). \quad (1)$$

The static component is given by:

$$F_{\text{stat}}(t) = \frac{1}{2}\gamma K_{\text{p}} S_{\text{stat}}^2 w, \tag{2}$$

where γ is soil unit weight, K_{p} is the passive earth pressure coefficient under critical state conditions, S_{stat} is the static debris flow height, and w is storage area width.

The dynamic component F_{dyn} is given by:

$$F_{\text{dyn}}(t) = k\rho v^2 A = k\rho v^2 S_{\text{dyn}} w, \tag{3}$$

where A is the impact area, k an empirical coefficient, ρ is the density of the flowing mass, v is the flow velocity, and S_{dyn} is the current debris flow height.

In the paper, 2D conditions have been considered (w equal to 1), and K_{p} and k have been considered equal to 3 and 5, respectively.

Moreover, assuming that debris flow is completely stopped by the sheltering structure, debris flow height and velocity vary with time and as a result, the application position of static and dynamic components of impact force changes along upstream face of sheltering structure.

The debris flow velocity and thickness strongly influence the value assumed by the impact force (Eq. 1). Indeed, extremely rapid debris flows generally show high values of dynamic component (Eq. 3) and smaller values of the static one (Eq. 2). When the velocity is lower, but yet compatible with that of rapid landslides, the static component (Eq. 2) assumes value higher than the dynamic one (Eq. 3). The maximum values reached by the debris flow thickness accumulated on the upstream side (impact side) of the structure and debris flow velocity and, as a result, the magnitude of impact force is strongly depending on these situations.

To consider the influence of the static and dynamic components on deformative response of sheltering structures, two cases, named case 1 (C1) and case 2 (C2), have been analyzed considering the debris flow velocity and thickness trends over time. Figure 2 shows debris flow height and velocity assumed for case 1 (C1) and case 2 (C2). In particular, the trend debris flow height–time was assumed equal for both considered cases (Fig. 2a), while two different trends of debris flow velocity–time (Fig. 2b) were assumed for the two different analyzed cases.

Case C1 is typical of debris flows characterized by a static component that is prevalent on the dynamic one (static dominant). It is assumed that, in C1, the value of the thickness mass deposited on the back of the sheltering structure over the time is regularly increasing, and at the final time (t_{f}), when it reaches the maximum value, it is equal to 3.0 m (Fig. 2a). In this case, the debris flow cinematic is characterized by two velocity peaks, the first one equal to 5 m/s and the second one equal to 4 m/s (Fig. 2b, blue line).

Case C2 is typical of debris flow with dynamic component that is prevalent to the static one (dynamic dominant). In this case, considering the same evolution of the thickness mass deposited over the time on the upstream face of the structure of static dominant case (Fig. 2a), the debris flow kinematic is characterized by two velocity peaks, the first one equal to 10 m/s and the second one equal to 6 m/s (Fig. 2b, red line).

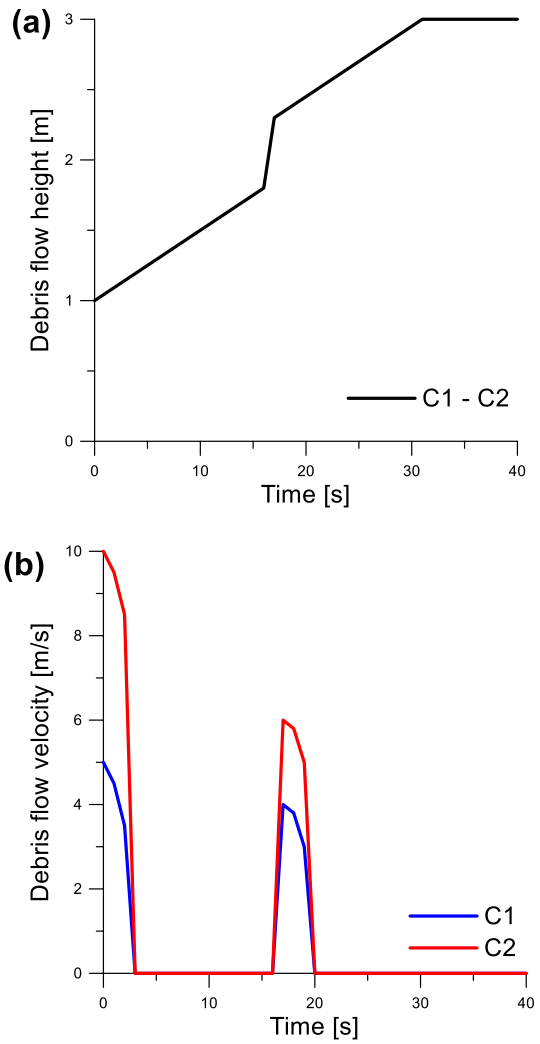

Fig. 2 Debris flow height **a** and velocity **b** assumed for two considered cases

Figure 3 shows the evolution of impact forces over time calculated by Eq. (1) in two considered cases considering the trends of debris flow height and velocity shown in Fig. 2. In particular, blue line refers to static dominant case (C1) and red line refers to dynamic dominant case (C2).

According to safe estimation of the peak impact force, the impact load is assumed to be completely transferred to the structure without dissipation and the stiffness and the inertial resistance of the artificial structure are neglected [15].

Because the debris flow height and velocity trends are known, the component F_{stat} and F_{dyn} trend has been calculated by Eqs. (2) and (3) and the application points on

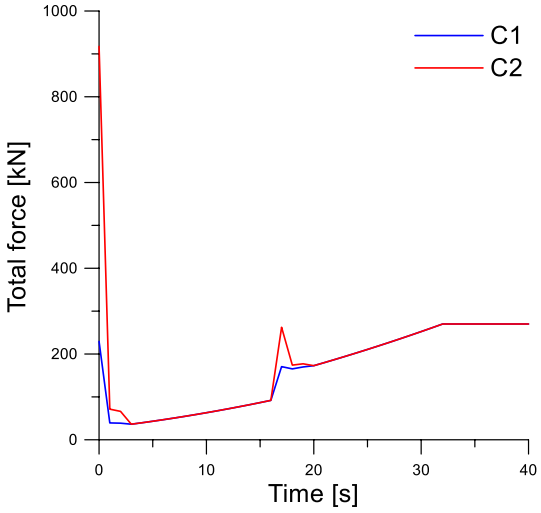

Fig. 3 Total force calculated in two analyzed cases

Table 1 Geometric features for different earth reinforced structures

Type	b [m]	B [m]	H [m]	α [°]	β [°]
R1	6.0	8.5	5.0	90°	63°
R2	6.0	11.0	5.0	63°	63°

the structure have been determined assuming a scheme of accumulation of material behind the obstacle.

An earth reinforced embankment has been considered as sheltering structure and the influence of different geometries of structure has also been investigated by means of FEM analyses considering two different embankments.

Table 1 summarizes geometric features of two structures. Figure 4 shows two earth reinforced structures that have been considered in the analysis, named type R1 and type R2.

The earth reinforced structures are both 5 m high and are reinforced by geogrids wrapped around the face with 0.50 m vertically spacing.

The type R1 structure has the upstream side (impact side) inclined 90° and the valley side inclined 63°. The top is 6 m width, and the base is 8.5 m large.

The type R2 structure has the upstream (impact side) and downstream sides inclined 63°. The top is 6 m width, and the base is 11 m large.

In the numerical analysis, a soil, classified as gravel with sand, has been considered both as filling material of earth structure and as soil foundation. Soil properties are summarized in Table 2.

Here γ is the unit weight of soil; c' is the cohesion; ϕ is the friction angle; ν is the Poisson coefficient; G_0 is the soil initial shear modulus.

The earth reinforced structure is made by HDPE extruded geogrid with a tensile modulus about equal to

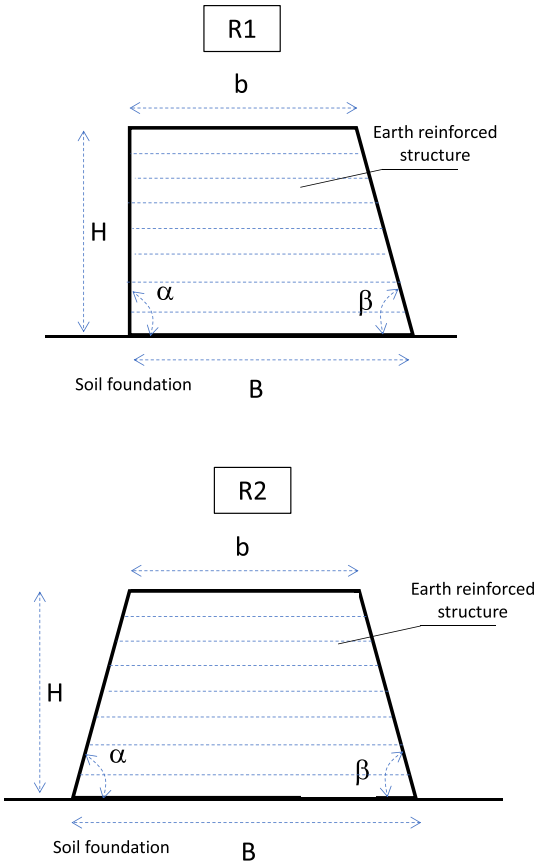

Fig. 4 Geometries of analyzed earth reinforced structures: type R1 and type R2

Table 2 Soil properties

γ [kN/m^3]	c' [kN/m^2]	φ [°]	ν [–]	G_0 [kN/m^2]
21	0.0	53	0.3	280

1200 kPa. Geogrids are one of the most common types of geosynthetics used for soil reinforcement. The use of geosynthetics has unique advantages over other soil strengthening techniques, due to technical, economic, and sustainability reasons (e.g., simplicity of construction, lower transportation costs, low emission, wide range of physical and mechanical properties, etc).

The redistribution of internal stresses within reinforced soil mass and its deformations depend on soil shear strength, reinforcement tensile strength and stiffness, and on interface stress mechanisms between soil and reinforcement. If the type of reinforcing material, geometrical shape, and mechanical properties change, the soil–geosynthetic interaction mechanisms vary. Therefore, the use of geosynthetics as reinforcement requires a clear understanding of soil–geosynthetic interaction behavior.

This interaction depends on the apparent interface coefficient of friction (μ) that can be obtained by pullout tests [16]. This coefficient has important implications on the design of geosynthetic reinforced structures.

In the numerical analysis performed, an average value equal to 0.9 has been used according to the experimental tests obtained by Moraci and Cardile [17] for the same interface (HDPE extruded geogrid—gravel with sand) considered in this paper.

Methods

The proposed approach for evaluating the deformative response of sheltering structures under the debris flow impact assumes that the accumulation behind the structure occurs and the structure is not overtopped by the flow (the height of impact is always lower than the height of the structure). By this way, it is possible to assess the distribution horizontal stress over time based on the scheme of accumulation of material behind the obstacle shown in Fig. 5 considering different impact times such as the first impact (t_0), impact at generic time (t), and final condition (t_f).

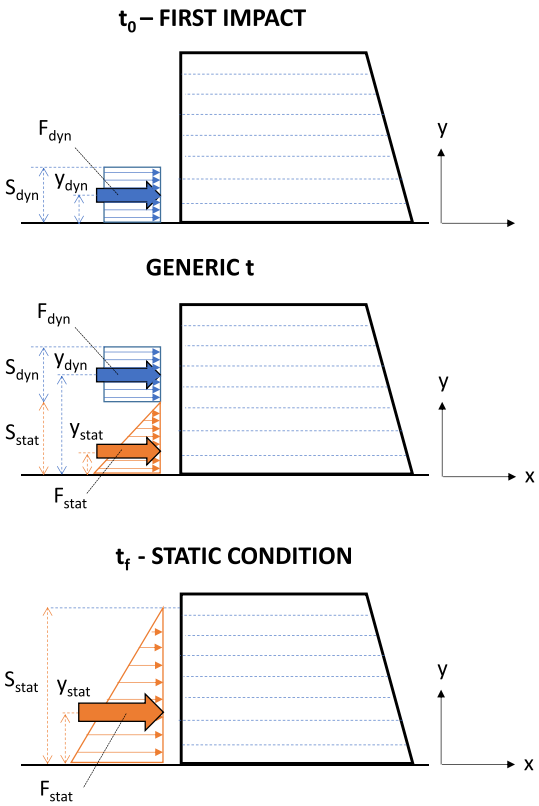

Fig. 5 Scheme of material accumulation and impact force distribution behind the structure

According to this scheme, the stress distribution due to the debris flow impact against obstacle is obtained by values of the following parameters varying during accumulation behind the obstacle: the dynamic component of impact force F_{dyn}, the thickness of dynamic component S_{dyn}, the application position of dynamic component Y_{dyn} assuming a rectangular stress distribution, the static component of impact force F_{stat}, the thickness of dynamic component S_{stat}, and the application position of static component Y_{stat} assuming a triangular stress distribution.

The method may be summarized as follows:

- Dynamic (F_{dyn}) and static (F_{stat}) impact force component evaluation for each time (i) of the impact using velocity (v) and height (h) trends of the debris flow behind the obstacle (e.g., obtained as output of numerical propagation analysis of debris flow with obstacle presence), according to the following expressions:

$$y_{\mathrm{dyn}_i} = h_{i-1} + \frac{\left(h_i - h_{i-1}\right)}{2} \tag{4}$$

$$S_{\mathrm{dyn}_i} = h_i - h_{i-1} \tag{5}$$

$$F_{\mathrm{dyn}_i} = k\rho v_i^2 A = k\rho v_i^2 S_{\mathrm{dyn}_i} w \tag{6}$$

$$y_{\mathrm{stat}_i} = \frac{h_{i-1}}{3} \tag{7}$$

$$S_{\mathrm{stat}_i} = h_{i-1} \tag{8}$$

$$F_{\mathrm{stat}_i} = \frac{1}{2}\gamma k_p S_{\mathrm{stat}_i}^2 w. \tag{9}$$

- Evaluation of the horizontal stress history (σ_x) for each point along upstream face of earth reinforced structure (ERS) as sum of two contributions (static and dynamic), assuming a triangular stress distribution for F_{stat} and a rectangular stress distribution for F_{dyn}:

$$\sigma_x(y,t) = \sigma_x(y,t)_{\mathrm{stat}} + \sigma_x(y,t)_{\mathrm{dyn}}, \tag{10}$$

where

$$\sigma_{\mathrm{hor}}(y,t)_{\mathrm{stat}} = \frac{2F_{\mathrm{stat}_i}}{S_{\mathrm{stat}_i}}\left(1 - \frac{y}{S_{\mathrm{stat}_i}}\right) \tag{11}$$

$$\sigma_{\mathrm{hor}}(y,t)_{\mathrm{dyn}} = \frac{F_{\mathrm{dyn}_i}}{S_{\mathrm{dyn}_i}}. \tag{12}$$

For example, referring to case 1 and earth reinforced structure R1, Fig. 6 shows horizontal stress distribution

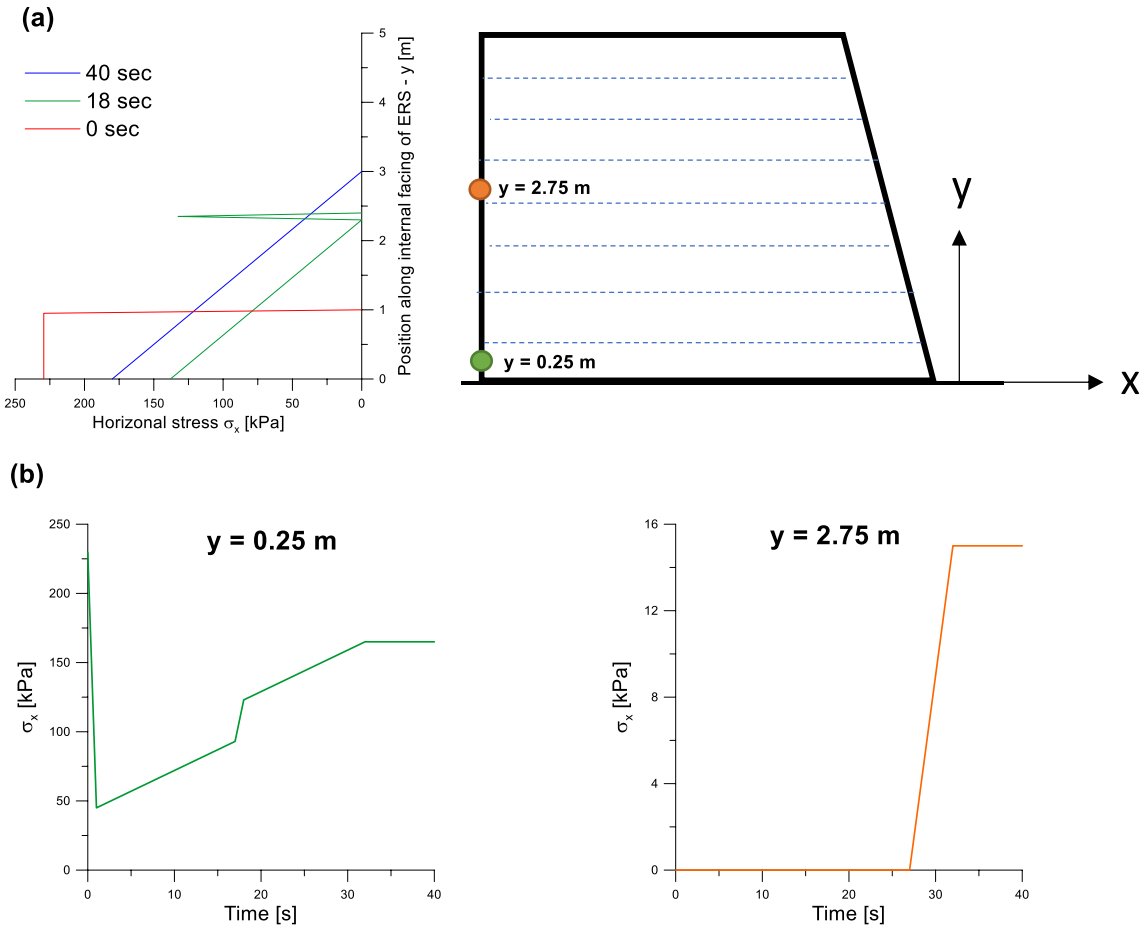

Fig. 6 Horizontal stress distribution at different time **a** and horizontal stress history at two points **b** along upstream face of earth reinforced structure

at different time t and horizontal stress history fortwo2 points along upstream face of earth reinforced structure.

- Assessment of the deformative response of earth reinforced structures by 2D FEM analysis using RS2-Geoscience [18], considering the stress histories (σ_h, t) along the upstream face previously obtained. In the paper, the analyses have been carried out using a triangular element mesh with the average size of the elements equal to 0.25 m with the smallest elements (about 0.15 m) along the geogrids and the upstream face. The suitability of the mesh adopted in the analysis has been verified through a mesh sensitivity analysis.

The FEM analyses were performed considering drained soil conditions. Different phases have been considered in the FEM analysis such as the initial stress conditions (equivalent to stage of construction of the structure), impact stress conditions (dynamic analyses), and final stress conditions. The soil has been considered as a linear elastic-perfectly plastic material and the soil strength parameters have been expressed in terms of shear strength angle and cohesion as reported in Table 2. To take into account soil nonlinear behavior, dynamic analyses have been performed considering the effect of confining pressure (σ'_0) and uniformity coefficient (C_u) on G/G_0 versus shear strain according to a simplified approach for shear-modulus degradation of compacted soils proposed by Rollins et al. [19]. The analyses have been carried out using values of G_0 equal to 280 MPa, σ'_0 equal to 100 kPa, and C_u equal to 20.

Geogrids were modeled by means of linear elastic and isotropic elements and as apparent interface coefficient of friction (μ) for the interface elements has been used that obtained by Moraci et al. (2014) for similar interfaces.

FEM Analyses Results and Discussion

FEM analyses results have been analyzed in terms of displacements obtained in different control points in the structures (Fig. 7) to catch the horizontal displacements in the upstream (impact side) and downstream faces and along a vertical section passing from the center of the top of earth reinforced structures.

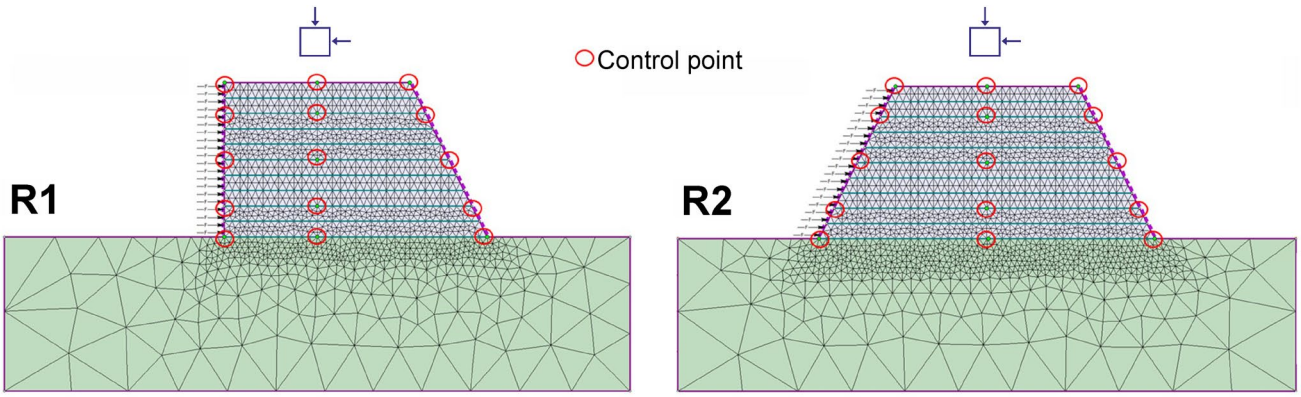

Fig. 7 FEM models: mesh and control points

Table 3 Numerically analyzed combinations

Embankment/flow	C1	C2
R1	R1–C1	R1–C2
R2	R2–C1	R2–C2

The numerically analyzed combinations in terms of dominant component of flow and geometry of embankment are summarized in Table 3.

The obtained results in terms of horizontal displacements for the considered structures in examined cases C1 (static dominant component) and C2 (dynamic dominant component) at the end of the impact are shown in Fig. 8.

The maximum horizontal displacements occur in the top of the structures and the structures slide predominantly over the base soil (Fig. 8). The maximum horizontal displacements (1.3×10^{-1} m and 2×10^{-1} m) occur when the dynamic component is larger than the static one for both structures (R1–C2 and R2–C2).

In the case R2–C2, it is possible to observe large horizontal displacements throughout the structure and the impact causes local displacements at the bottom upstream

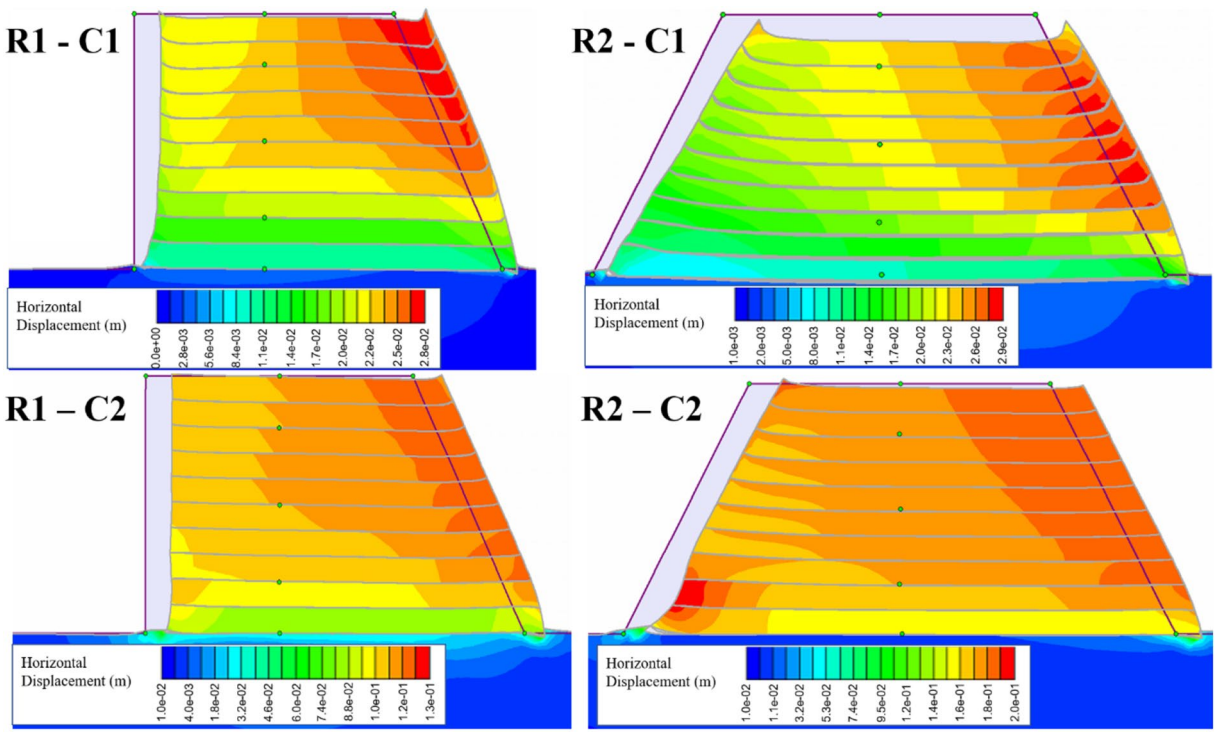

Fig. 8 Horizontal displacements obtained by numerically analyzed combinations

face near the base similar to impact occurring for individual boulders (Fig. 8).

Figure 9 shows the trend of the maximum horizontal displacement over time at control point C (located in the downstream top of embankments) in the two considered cases (C1 and C2) for the structures (R1 and R2).

From Fig. 9, it can be noticed that horizontal displacements increase over time immediately after the first impact ($t=0$), then they decrease and subsequently increase again. Moreover, larger horizontal displacements occur when the flow has a prevalent dynamic component C2 (dashed lines in the figure) and the maximum values are obtained for the combination R2–C2. Besides, in the case of flow with a prevalent dynamic component (C2), there are relevant differences between the horizontal displacements obtained for earth reinforced structure R2 (red line) and those for earth reinforced structure R1 (blue line). On the contrary, in the case of flow with a prevalent static component C1 (solid lines in Fig. 9), the displacements are larger in earth reinforced structure R1 than those in earth reinforced structure R2 and they are not very different.

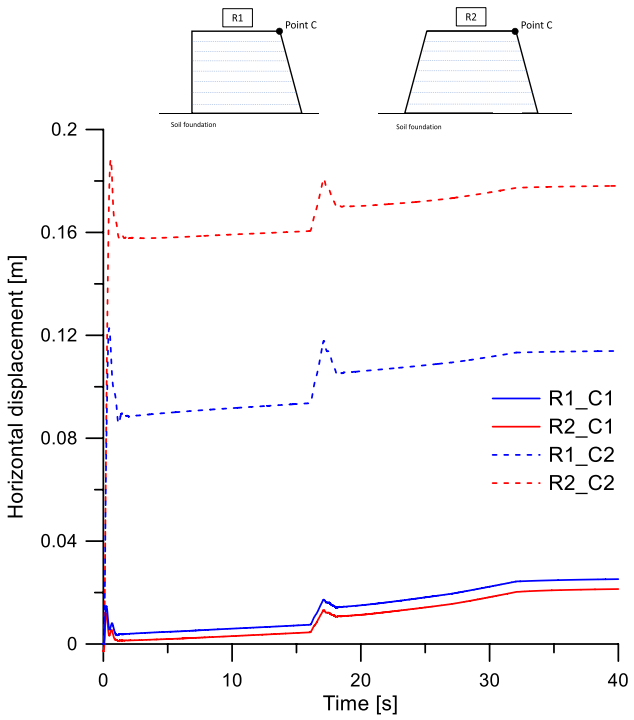

Fig. 9 Maximum horizontal displacement (point C)

Figure 10 shows the trend of the average horizontal displacement over time at the base of the embankments (R1 and R2) in the two considered cases (C1 and C2).

It can be noticed that the horizontal displacements increase immediately after the first impact (t = 0), then decrease and subsequently increase with peaks less evident than those observed at the top of structures (Fig. 9).

The largest horizontal displacements occur when the flow is with prevalent dynamic component C2 (dashed lines in the Figure) and are maximum in the case of the structure with internal inclined side (R2). Moreover, in the case C2, there are differences between horizontal displacements recorded for R2 and those recorded for R1. In the case of the prevalent static component C1 (solid lines), the differences between the displacements are low or null (R1–C1 and R2–C1).

Figure 11 shows the trend of horizontal displacements with depth along three sections upstream face (impact side) (Fig. 11a), vertical section passing from the center of the top of earth reinforced structure (Fig. 11b) and downstream face (Fig. 11c) of embankment 1 at different times, immediately

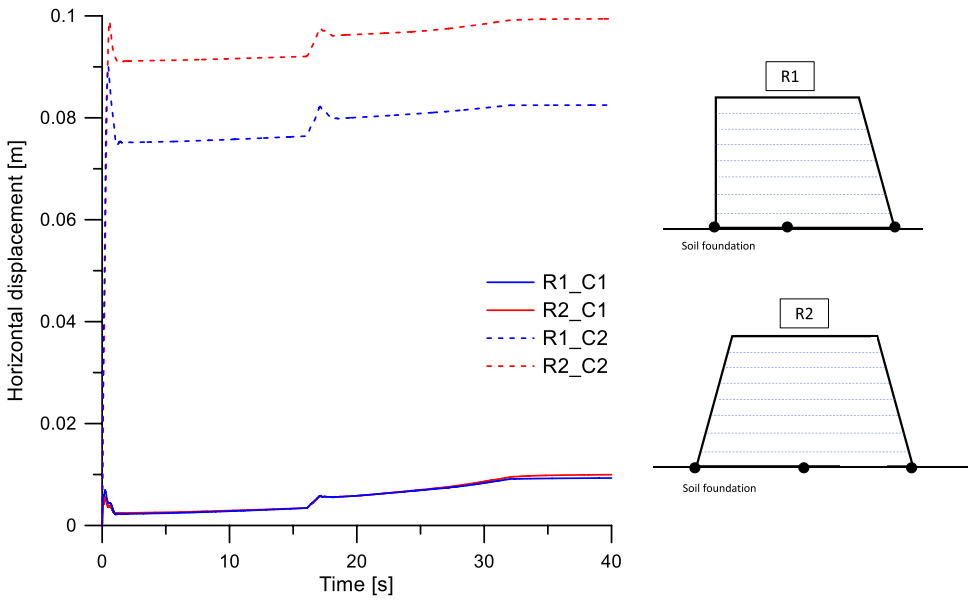

Fig. 10 Average horizontal displacement at the base of the structures

after the impact (t = 1 s), at second impact (18 s), at the end of the process (40 s) in the two flow conditions considered C1 and C2.

It can be noted that horizontal displacements are always larger in case C2 (red lines) than those of case C1 (blue lines). The displacements decrease moving from the top to the base of the structure and in the case C2 at $t = 1$ s, the structure already slided significantly over the base soil in all considered sections. At the same time, the difference between the horizontal displacements in the three considered sections is reduced at the base of the embankment (z = 5 m).

The maximum value of horizontal displacement (equal to 0.119 m) is reached at 2.5 m (40 s case C2) in the downstream face of structure (Fig. 11c).

Figure 12 shows the trend of horizontal displacements with depth in the two considered flow conditions C1 and C2 along three sections upstream (Fig. 12a), vertical section passing from the center of the top of earth reinforced structure (Fig. 12b) and downstream faces (Fig. 12c) of embankment 2 at different times, immediately after the impact (t = 1 s), at second impact (18 s), at the end of the process (40 s).

It can be noted that horizontal displacements are always larger in case C2 (red lines) than those of case C1 (blue lines). Regardless the flow conditions, as time varies, the values obtained immediately after the impact (t = 1 s) are slightly different from those obtained at the end of the impact (40 s), thus highlighting that the most important displacements occur immediately after the first impact.

In case C1, the displacements increase in the three sections considered as time increases. At the same time, the reached horizontal displacements are generally greater in the first 4 m of depth and are reduced at the base (z = 5 m).

In case C2, the structure already slided significantly over the base soil in all considered sections. The upstream section is the most stressed at 4 m considering the type of impact that the flow C2 produces (similar to the impact of a block); here the maximum value of horizontal displacement is reached at 4 m (at 40 s) and it is equal to 0.190 m (Fig. 12a). This value also is the maximum one obtained in all performed simulations.

Figure 13 shows the trend of the horizontal displacements along the vertical section passing from the center of the top of earth reinforced structures (R1 and R2) due to the flow to the dominant static component (C1) at different times immediately after the impact ($t = 1$ s), at intermediate time (t = 18 s), and at the end of the impact (40 s).

It can be noted that in case C1, there are generally small differences of displacements along the vertical sections passing from the center of the top of two earth reinforced structures and the differences become evident especially at the top rather than at the base. In particular, at the end of the process (40 s) at the base, there are greater displacements in the case

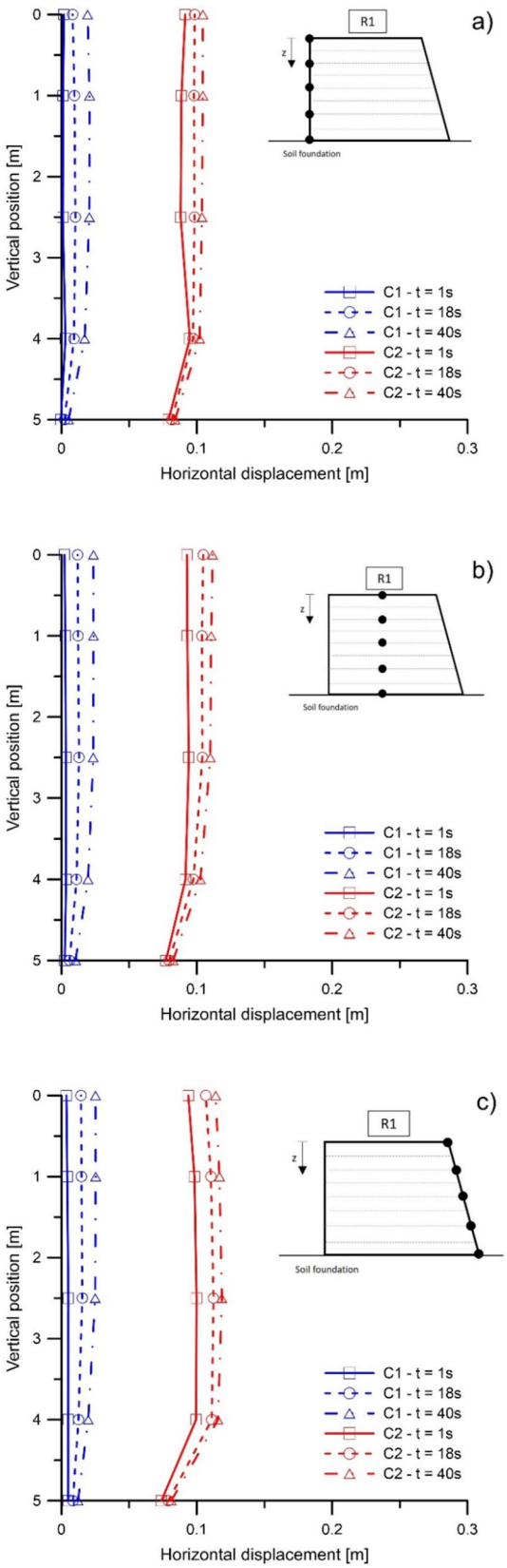

Fig. 11 Horizontal displacements along the sections of structure R1. **a** upstream face; **b** vertical section passing from the center of the top; **c** downstream face

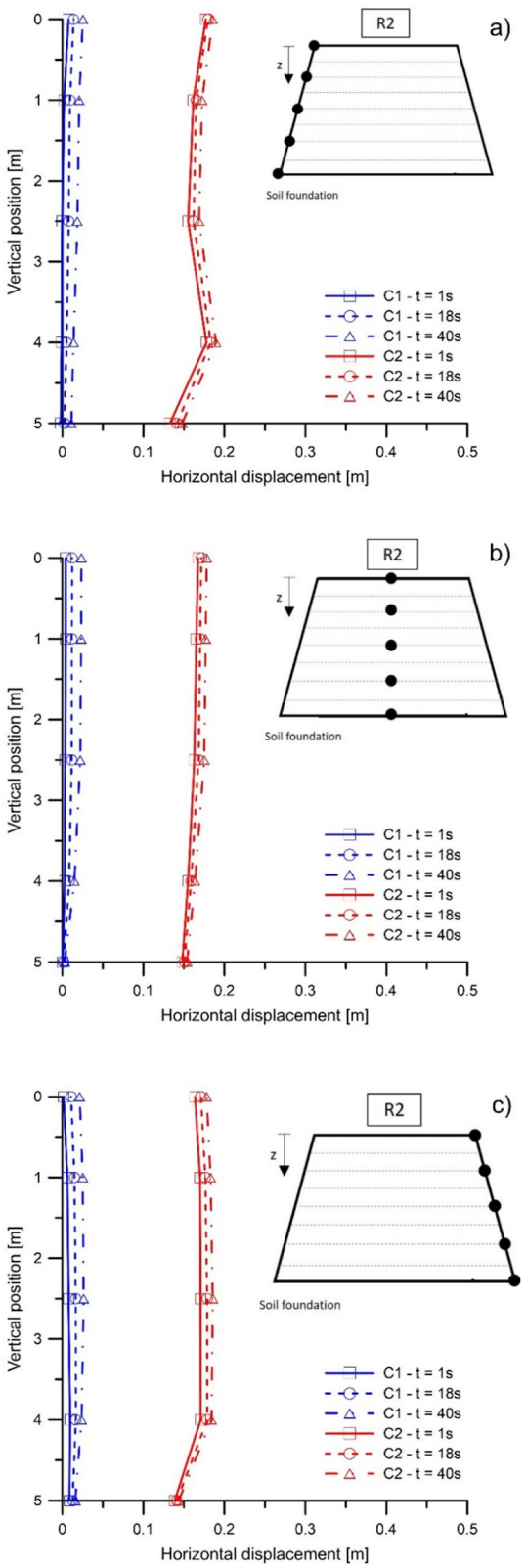

Fig. 12 Horizontal displacements along the sections of structure R2. **a** upstream face; **b** vertical section passing from the center of the top; **c** downstream face

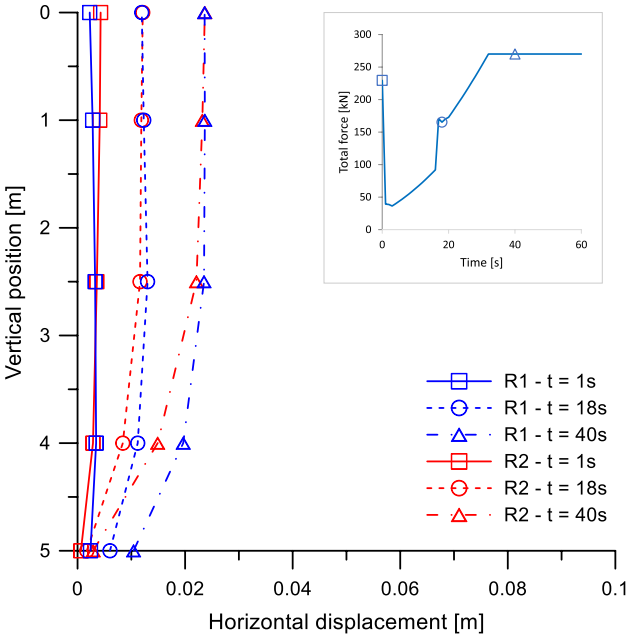

Fig. 13 Horizontal displacement in the vertical section passing from the center of the top of two earth reinforced structures R1 and R2 for case 1 (C1)

of the structure R1 (horizontal displacement = 0.013 m) than those of the structure R2. The maximum displacements are equal to 22 mm at 40 s.

Figure 14 shows the trend of the horizontal displacements along the vertical section passing from the center of the top of two earth reinforced structures R1 and R2 due to the dominant dynamic component flow (C2) at different times immediately after the impact (t = 1 s), at intermediate time (t = 18 s), and at the end of the process (40 s).

Figure 14 shows that when the dynamic component is prevalent, the greatest horizontal displacements (0.16 m) are obtained along the vertical section passing from the center of the top of earth reinforced structure with an upstream inclined face (R2). Besides, a translational sliding similar to the sliding of a rigid block in the embankment with a vertical face (R1) at the base is evident.

Conclusion

The paper proposed a novel approach to evaluate the impact stress against deformable sheltering structure at any instant of time of the phenomenon along the upstream face height of the structure depending on the dominant flow component. For this purpose, different deformative mechanisms of earth reinforced embankments have been observed for the analyzed combinations of flow and embankment. The main conclusions can be summarized as follows.

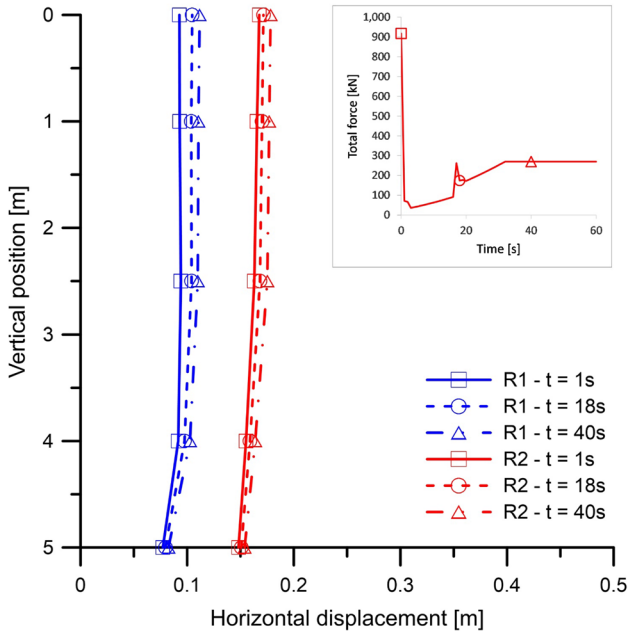

Fig. 14 Horizontal displacement in the vertical section passing from the center of the top of two earth reinforced structures R1 and R2 for case 2 (C2)

- The reinforced structure slides over the base soil when the dynamic component of impact force is prevalent respect to the static one. Local displacements have been observed near the bottom of upstream face of R2 structure similar to those due to impact of individual boulders in the combination R2–C2.
- Flows characterized by a dynamic component that is prevalent to the static one (C2) (dynamic dominant) provided in all analyzed cases the highest horizontal displacements independently on type of considered structure.
- In the C2 case, the variation of horizontal displacements along the vertical sections passing from the center of the top of earth reinforced structures R1 and R2 over the time has shown that the history of the impact forces causes large horizontal displacements (in the range 0.07–0.19 m) that are maximum at the top and minimum at the base (Figs. 11, 12). It has been observed that the larger amount of the displacements occurs already at the moment of the first impact (at $t = 1$ s).
- In the C1 case, the variation of displacements along the vertical sections passing from the center of the top of earth reinforced structures R1 and R2 over the time showed that the history of the impact forces causes small horizontal displacements (ranging from 0 to 0.03 m). Also in this case, the maximum horizontal displacements occur at the top while the minimum value is at the base. Moreover, in the case of flow with dominant static component (C1), at the same instant of time, there are no differences in the horizontal displacements at the top of two different structures (R1 and R2) while these displacement differences increase with the depth and become maximum at the base (Fig. 13). Therefore, in the case of a dominant static component, the geometry of the embankment has negligible effects on the horizontal displacements. As shown by the small displacements observed at the base (less than 0.01 m), sliding does not occur at the base of the embankments (R1 and R2).
- In the case of the dominant dynamic component (C2), at every instant of time, there are significant differences in the horizontal displacements due to the geometry of the embankment (R1 or R2) (Fig. 14). In this case, a sliding has been observed at the base for both the analyzed geometries (R1 and R2) with large displacement ranging from 0.075 m (R1) to 0.15 m (R2). The greatest horizontal displacements are obtained along the vertical section passing from the center of the top of earth reinforced structure with an upstream inclined face (R2). Therefore, in the case of dominant dynamic component, the deformative response is strongly dependent on the embankment geometry.
- The results obtained by numerical analyses have provided useful indications on the importance of the geometry of the structure and of type dominant component of impact force on the displacement response of a reinforced embankment subjected to a flow impact.

Finally, the design of sheltering structures in exposed areas represents a societal relevant aspect and the results obtained in this study in the analyzed cases have provided important knowledge for the design of mitigation structures in such areas.

Author Contributions DG, MCM, and NM contributed to the conceptualization and design of analyses. DG, MCM, and MC conducted all the analyses. DG, MCM, MC, and NM analyzed and interpreted all the test results. DG, MCM, MC, and NM wrote the original draft, and NM contributed to editing and supervising. All authors read and approved this manuscript.

Funding Open access funding provided by Università degli Studi di Salerno within the CRUI-CARE Agreement. This work was partially funded by the Next Generation EU—Italian NRRP, Mission 4, Component 2, Investment 1.5, call for the creation and strengthening of 'Innovation Ecosystems', building 'Territorial R&D Leaders' (Directorial Decree n. 2021/3277)—project Tech4You—Technologies for climate change adaptation and quality of life improvement, n. ECS0000009. This work reflects only the authors' views and opinions, neither the Ministry for University and Research nor the European Commission can be considered responsible for them.

Data Availability Data generated or analyzed during this study are available from the corresponding author upon reasonable request.

Declarations

Conflict of Interest The authors declare that they have no competing interests.

References

1. Hungr O, Morgan GC, Kellerhals R (1984) Quantitative analysis of debris torrent hazards for design of remedial measures. Can Geotech J 21(4):663–677
2. Thouret JC, Antoine S, Magill C, Ollier C (2020) Lahars and debris flows: characteristics and impacts. Earth Sci Rev 201:103003
3. Ciurleo M, Mandaglio MC, Moraci N (2019) Landslide susceptibility assessment by TRIGRS in a frequently affected shallow instability area. Landslides 16:175–188
4. Ciurleo M, Mandaglio MC, Moraci N (2021) A quantitative approach for debris flow inception and propagation analysis in the lead up to risk management. Landslides 18:2073–2093
5. Geotechnical Control Office (GCO) (1988) Geoguide 3: guide to rock and soil descriptions. Civil Engineering Services Department, Hong Kong
6. Armanini A (1997) On the dynamic impact of debris flows. Recent developments on debris flows. Springer, Berlin, pp 208–226
7. Arattano M, Franzi L (2003) On the evaluation of debris flows dynamics by means of mathematical models. Nat Hazards Earth Syst Sci 3(6):539–544
8. Suda J, Hübl J, Bergmeister K (2010) Design and construction of high stressed concrete structures as protection works for torrent control in the Austrian Alps. In: Proceedings of the 3rd International FIB Congress, Washington, DC
9. Gioffrè D, Mandaglio MC, di Prisco C, Moraci N (2017) Evaluation of rapid landslide impact forces against sheltering structures. Ital Geotech J 51(3):64–76
10. Calvetti F, di Prisco CG, Vairaktaris E (2017) DEM assessment of impact forces of dry granular masses on rigid structures. Acta Geotech 12:129–144
11. Di Perna A, Cuomo S, Martinelli M (2022) Empirical formulation for debris flow impact and energy release. Geoenviron Disasters 9(8):1–17
12. Cuomo S, Di Perna A, Martinelli M (2022) design protection barriers against flow-like landslides. Progress Landslide Res Technol 1(1):123–136
13. He S, Li X, Liu W (2016) Prediction of impact force of debris flows based on distribution and size of particles. Environ Earth Sci 75(4):297–298
14. Kwan J, Sze E, Lam C (2019) Finite element analysis for rockfall and debris flow mitigation works. Can Geotech J 56(9):1225–1250
15. Vagnon F, Segalini A (2016) Debris flow impact estimation on a rigid structure. Nat Hazard 16(7):1691–1697
16. Moraci N, Cardile G, Gioffrè D, Mandaglio MC, Calvarano LS, Carbone L (2014) Soil geosynthetic interaction: design parameters from experimental and theoretical analysis. Transport Infrastr Geotechnol 1(2):165–227. https://doi.org/10.1007/s40515-014-0007-2. (**Ed.Springer.OnlineISSN2196-7210. ScopusIndex=2-s2.0-85012816482**)
17. Moraci N, Cardile G (2012) Deformative behaviour of different geogrids embedded in a granular soil under monotonic and cyclic pullout loads. Geotext Geomembr 32:104–110 (**ISSN: 0266-1144**)
18. RS2 Manual (2022) Documentation and Theory Overview. Rocscience www.rocscience.com. Accessed 18 Oct 2023
19. Rollins KM, Singh M, Roy J (2020) Simplified equations for shear-modulus degradation and damping of gravels. J Geotech Geoenviron Eng ASCE,. https://doi.org/10.1061/(ASCE)GT.1943-5606.0002300